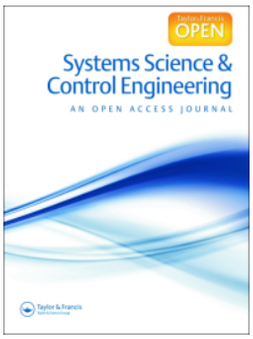

Taylor & Francis
Taylor & Francis Group

Systems Science & Control Engineering

An Open Access Journal

ISSN: (Print) (Online) Journal homepage: www.tandfonline.com/journals/tssc20

Second order sliding mode control with proportional integral observer for wing rock

Ahmad Mahmood & Jamshed Iqbal

To cite this article: Ahmad Mahmood & Jamshed Iqbal (2025) Second order sliding mode control with proportional integral observer for wing rock, Systems Science & Control Engineering, 13:1, 2460427, DOI: 10.1080/21642583.2025.2460427

To link to this article: https://doi.org/10.1080/21642583.2025.2460427

© 2025 The Author(s). Published by Informa UK Limited, trading as Taylor & Francis Group.

Published online: 06 Feb 2025.

Submit your article to this journal

View related articles

View Crossmark data

Full Terms & Conditions of access and use can be found at
https://www.tandfonline.com/action/journalInformation?journalCode=tssc20

SYSTEMS SCIENCE & CONTROL ENGINEERING: AN OPEN ACCESS JOURNAL
2025, VOL. 13, NO. 1, 2460427
https://doi.org/10.1080/21642583.2025.2460427

Taylor & Francis
Taylor & Francis Group

OPEN ACCESS Check for updates

Second order sliding mode control with proportional integral observer for wing rock

Ahmad Mahmood[a] and Jamshed Iqbal[b]

[a]School of Engineering, Electrical Engineering Department, University of Management and Technology, Lahore, Pakistan; [b]School of Computer Science, Faculty of Science and Engineering, University of Hull, Hull, UK

ABSTRACT
In this study, a reduced-order fast proportional integral (PI) observer with a fast convergence function based on the equivalent control notion is developed to estimate the side slip angle β. An unknown state can be discovered by forcing the PI term on the state error, which is the difference between the real and estimated states. A second order sliding mode control (SOSMC) based on a proposed nonlinear sliding manifold is designed to achieve improved transient response and control performance by robustness. The proposed sliding manifold ensures the convergence of the roll angle in finite time. To validate the assertion regarding the proposed SOSMC, classical SOSMC and proportional integral derivative (PID) SOSMC are simulated both in the absence and presence of disturbances. The simulation results show that the proposed SOSMC over-performs in terms of achieving the desired response in both cases. Additionally, a numerical analysis is also performed for both scenarios to evaluate the effectiveness of the proposed controller in terms of the power consumption of the control law and burden on the aileron control surface. Finally, Monte Carlo simulations are performed to demonstrate the robustness of the proposed controller against external disturbances.

ARTICLE HISTORY
Received 22 August 2024
Accepted 26 January 2025

KEYWORDS
Wing rock; proportional integral observer; equivalent control sliding manifold; second order sliding mode control

1. Introduction

To meet the demands of aerial dominance, modern aircraft and jet aircraft are designed for high speed, high angles of attack and manoeuverability. These criteria require aircraft to operate with a low aspect ratio, a high swept-back or delta wing and a long slender body, resulting in exceedingly complicated aircraft dynamics in nonlinear flying regimes, and an increase in maximum possible speeds owing to drag reduction (Ghorawat, 2015). Flying at low speeds (subsonic, transonic) with a high swept back or delta wing necessitates relatively high angles of attack, which induces a characteristic vortical flow, and these geometric configurations provide more longitudinal stability than lateral stability (Pakmehr, 2005). Thus, weak lateral stability reduces the rolling inertia, and any form of perturbation may result in instability under a high swept back or delta wings. Whenever a lateral perturbation occurs, the vortical flow begins to interact with the aircraft body, causing oscillations, predominantly in roll, that vary with variations in the angle of attack. This leads to damped oscillations at low angles of attack, but diminished damping at high angles of attack, resulting in a limit cycle. Hence the appearance of a limit cycle along the roll channel is called the Wing Rock Phenomenon (WRP), as illustrated in Figure 1. The WRP is further classified as slender wing rock, conventional wing rock and wing body rock according to the intricacy of its interaction with rigid body motion (Saad, 2000).

To eliminate WRP, feedback control that ensures stability and maintains aircraft performance is essential. Based on the uncertainties generated by aerodynamic factors and unknown disturbances, Yin et al. (2019) formulated two control schemes for the aircraft to reduce wing rock motion. The first scheme employs adaptive control to estimate all unknown rolling coefficients and an observer is used in the second scheme to evaluate uncertainties such as parameters perturbation and external disturbances. To eliminate wing rock oscillations and track the roll angle of a linear referenced model, Andrievsky, Kudryashova, Kuznetsov, Kuznetsova, Tomashevich et al. (2019) and Andrievsky, Kudryashova, Kuznetsov and Kuznetsova (2020) proposed an adaptive control based on an implicit reference model. They also improved the adaptive control strategy by taking into account the coupling relationship between roll and side slip motion, as well as the constraints on aileron deflection. To deal with WRP in the presence of matched uncertainty, Roshanian and Rahimzadeh (2021) suggested

CONTACT Jamshed Iqbal j.iqbal@hull.ac.uk, iqbal.jam@gmail.com

© 2025 The Author(s). Published by Informa UK Limited, trading as Taylor & Francis Group.
This is an Open Access article distributed under the terms of the Creative Commons Attribution License (http://creativecommons.org/licenses/by/4.0/), which permits unrestricted use, distribution, and reproduction in any medium, provided the original work is properly cited. The terms on which this article has been published allow the posting of the Accepted Manuscript in a repository by the author(s) or with their consent.

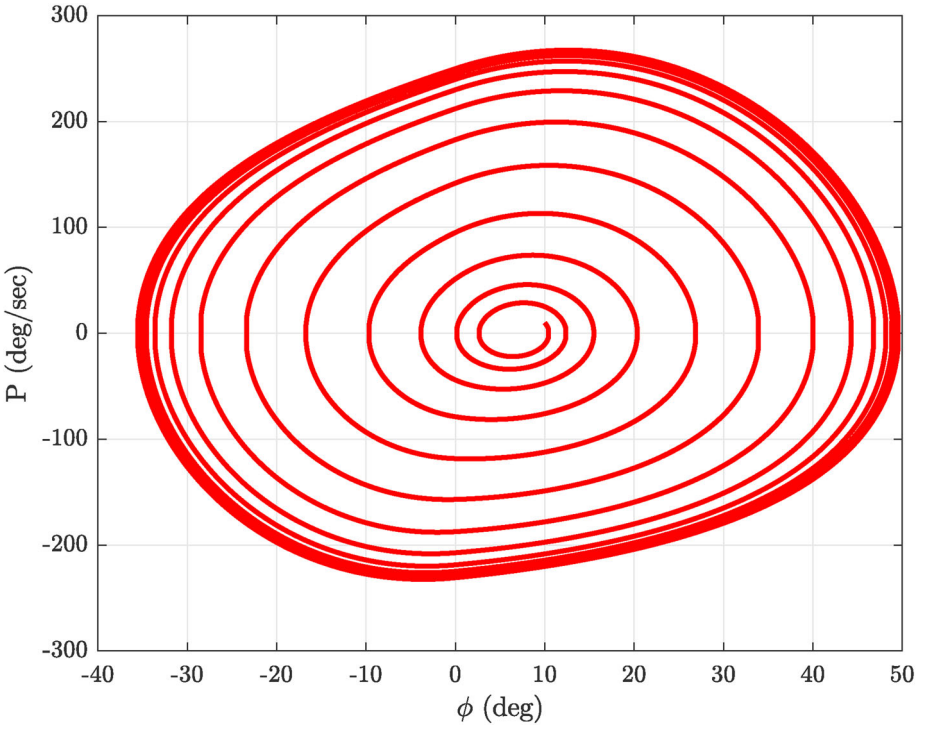

Figure 1. Wing Rock Phenomenon (Zribi et al., 2013).

model reference adaptive control with an integrator term, and they composed the adaptive laws with exponential quadratic terms incorporating a novel quadratic Lyapunov function. Ene (2013) deployed an adaptive backstepping control strategy to realize the parameters as well as stabilize the wing rock oscillations. Malekzadeh, Khosravi et al. (2015) sought to deal with the high oscillations along the roll axis of aircraft at high angles of attack by developing the conventional backstepping control technique. For dealing with wing rock variations, D. Wu et al. (2017) reported a robust adaptive backstepping control approach and an adaptive radial basis function neural network to predict the uncertainty of the wing rock system. An auxiliary system is offered as well to deal with the actuator saturation problem during backstepping control, and a dynamic surface control strategy is introduced to avoid the complicated computation of virtual control derivatives that occur in backstepping control.

Midhat (2017) presented a comparison of linear quadratic regulator (LQR) and min–max control schemes to deal with the WRP and redesigned the LQR controller for the disturbance environment. To prevent wing rock motion, Kuperman and Zhong (2015) developed a robust control strategy based on the uncertainty and disturbance estimation. Malekzadeh, Sadati et al. (2016) incorporated a proportional integral derivative (PID) controller to stabilize the wing rock limit cycle, and proposed a wavelet neural network-based auto mechanism to adjust the PID control design gains. To reduce the influence of wing rock motion, Abdul-Kareem et al. (2022) proposed linear and nonlinear active disturbance rejection control methods as well as a butterfly optimization approach to optimize the gains of both controllers. A Lyapunov-based full states feedback approach with parametric uncertainties compensation is designed in Ibrir and Su (2014) to stabilize wing rock dynamics. Immersion and invariance based adaptive control to stabilize the wing rock motion is presented in Lee and Singh (2017). To achieve finite time convergence along the roll angle, a nonlinear terminal manifold is designed. To estimate the parameters, an adaptive control law is designed with frozen capability, which implies that once the estimated parameter reaches the measured parameter, it remains the same throughout the time and further truncates the estimation process. Cao et al. (2006) developed an $\mathcal{L}_1$ adaptive control scheme to handle WRP in the presence of uncertainties and disturbances. To address the sensitivity of roll moment coefficients at different angles of attack and WRP, Xin and Balakrishnan (2004) operated the $\theta - D$ suboptimal control and solved the optimality problem to obtain the wing rock suppression by introducing a perturbation into the Hamilton–Jacobi–Bellman equation.

Intelligent approaches such as fuzzy logic and neural networks are capable of performing in situations where plant information is inaccurate and operating conditions are uncertain. To address the WRP of delta wing aircraft, fuzzy logic-based control, fuzzy PD control and an upgraded version of fuzzy PD control, variable universe

fuzzy control, are employed in Sreenatha et al. (2000) and Z.L. Liu et al. (2003, 2004). A single hidden layer-based adaptive neural network controller (Calise et al., 2004), and an L_2 adaptive controller with a recurrent neural network identifier (Hsu et al., 2005) are developed to cope the wing rock oscillations. Lin and Hsu (2004) developed a supervisory recurrent fuzzy neural network to control a wing rock system, and employed a recurrent fuzzy neural network to adaptively simulate a linear reference model.

To eliminate wing rock oscillations by cancelling out the roll angle error, Guglieri and Sartori (2013) proposed a conventional Sliding Mode Control (SMC) and analysed the parametric uncertainties of the wing rock model, which varied dynamically with the angle of attack. The backstepping SMC and disturbance observer-based backstepping SMC are presented in Humaidi et al. (2019) to deal with wing rock motion and disturbances. To dampen the wing rock motion in a delta wing aircraft, Al-Qassar et al. (2021) constructed a supertwisting SMC, and utilized a heuristic optimization approach, specifically the whale optimization algorithm, to compute the optimal gains of the supertwisting SMC, and then compared the results of both controllers to verify the superiority of the optimal supertwisting SMC. Based on state transformation, feedback linearization control and classical SMC methodologies are developed in Zribi et al. (2013) to convert the wing rock model into a controlled companion form to stabilize the fluctuations of the delta-wing aircraft along the roll axis. The asymptotic error convergence of both controllers is explored through simulations, and it is found that feedback linearization demonstrates a faster convergence than SMC. However, there is a disadvantage in the form of an undershoot when the roll angle is stabilized. In the presence of time-varying uncertainties, an intelligent control strategy based on type-2 fuzzy logic and the SMC technique is developed by Tao et al. (2012) to suppress wing rock and track the intended roll angle. To estimate the rolling function, an extended sequential adaptive fuzzy inference system is constructed. Furthermore, after estimating the function, SMC-based law is developed to compensate for the error introduced by the fuzzy technique and manage the WRP in Rong et al. (2014). The dutch-roll mode oscillations of delta-wing aircraft are suppressed by SMC in Z. Liu and Svoboda (2003) and to handle the imprecision of Dutch roll dynamics, a fuzzy logic control is integrated with SMC. The chain of integrator control approach is implemented in D.W. Wu et al. (2014) to solve the problem of wing rock stability in the presence of disturbances, and a higher order sliding mode disturbance observer is proposed to handle the disturbances during wing rock motion.

Following the aforementioned exhaustive literature review on WRP, much of this research focuses on the adaptive formulations and parameter estimation of wing rock models. Some attention is given to the effectiveness and convergence behaviour, as well as the state estimation. Consequently, it is crucial to develop a nonlinear controller that can suppress the WRP and exhibit a satisfactory convergent behaviour and transient response, while accounting for disturbances and incorporating state estimation. The main contributions of this study in WRP suppression are as follows:

- Extended state observers (Fan et al., 2023), high gain observers and sliding mode observers are full state observers. If only one state has to be estimated, a reduced-order observer is designed. A reduced-order sliding mode observer (ROSMO) (Mahmood & Okasha, 2024) offers an attractive state estimation capability, but it has the significant disadvantage of chattering. To prevent chattering from ROSMO, a low-pass filter is introduced, which also depends on the switching frequency and frequency of the system dynamics. Based on the notion of equivalent control (V. Utkin, Poznyak, Y.V. Orlov et al., 2020), a reduced-order fast proportional integral (ROFPI) observer is proposed that takes into account these obstacles and estimates the side slip angle.
- To steer the state of the wing rock system to its intended set point or reference signal with a satisfactory transient response, a nonlinear sliding manifold based on the *tanh* function is developed. Furthermore, in the presence of an external disturbance, the control law based on the suggested sliding manifold ensures the control efficacy in terms of less power consumption and stress on the control surface.
- The ROFPI observer and reduced-order proportional integral (ROPI) observer without the convergence function are compared to evaluate the convergence performance. In addition, the efficiency of the SOSMC in suppressing the WRP is characterized by a simulation comparison with classical SOSM and PID SOSMC, and the closed-loop stability of the SOSMC is established by the Lyapunov theory.

The rest of the manuscript is organized as follows: Section 2 explains the wing rock dynamics and objective formulation for controller design. The observer design and SOSMC controllers are described in Section. 3. Section 4 presents simulation results for the classical, PID, and proposed SOSMC schemes, as well as Monte Carlo simulations. Finally, the paper is concluded in Section 5.

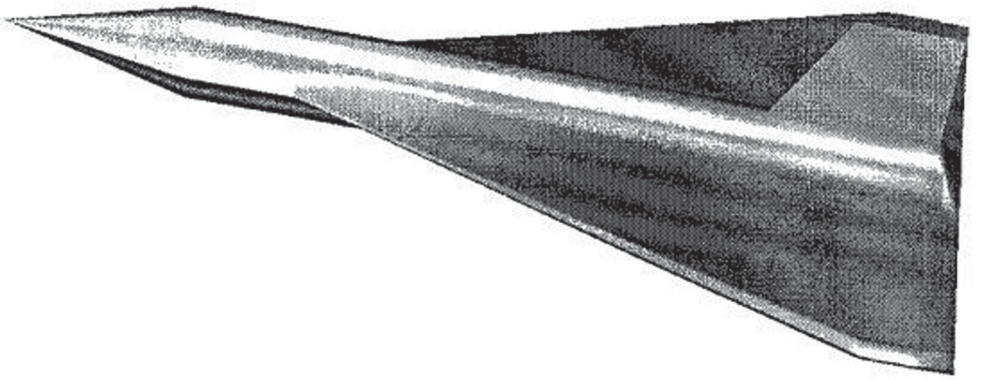

Figure 2. Delta wing configuration aircraft (Saad, 2000).

2. Wing rock modelling and problem formulation

Wing rock is normally represented as a self-induced, pure rolling motion, characterized by the rolling moment being a nonlinear function of the roll angle ϕ, and the roll rate P. A wing rock dynamic model of a delta wing configuration aircraft as shown in Figure 2 has been described in Ghorawat (2015), Tewari (2000), and the following assumptions are taken into account.

Assumption 2.1: The nonlinear terms of β are smaller than the ϕ.

To obtain pure rolling dynamics, sideslip dynamics is incorporated into the model by permitting a yaw motion. Thus, the rolling moment can be formulated as:

$$\mathcal{I}_{\mathcal{XX}}\ddot{\phi} = \mu\dot{\phi} + \mathcal{C}_{\tilde{\beta}}\beta - \mathcal{C}_{\tilde{R}}\dot{\beta} + \mathcal{C}_{\tilde{\delta}_a}\delta_a + \mathcal{F}(\phi,\dot{\phi}) \quad (1)$$

where $\mathcal{I}_{\mathcal{XX}}$ is the moment of inertia about the X-axis, μ is the sting damping coefficient, and $\mathcal{C}_{\tilde{\beta}}, \mathcal{C}_{\tilde{R}}$, and $\mathcal{C}_{\tilde{\delta}_a}$ are the coefficients of the sideslip angle, yaw rate and aileron deflection respectively. $\mathcal{F}(\phi,\dot{\phi})$ is a nonlinear self-induced rolling function and is written as:

$$\mathcal{F}(\phi,\dot{\phi}) = \mathfrak{a}_1\phi + \mathfrak{a}_2\dot{\phi} + \mathfrak{a}_3\dot{\phi}^3 + \mathfrak{a}_4\phi^2\dot{\phi} + \mathfrak{a}_5\phi\dot{\phi}^2 \quad (2)$$

where $\mathfrak{a}_i$, $i \in \{1, 2, \ldots, 5\}$ is computed from the experimental data at a certain angle of attack. Decomposing (1) yields the roll angle ϕ and roll rate P as follows:

$$\dot{\phi} = P \quad (3)$$

$$\begin{aligned}\dot{P} &= \frac{1}{\mathcal{I}_{\mathcal{XX}}}(\mathfrak{a}_1\phi + \mathfrak{a}_2P + \mathfrak{a}_3P^3 + \mathfrak{a}_4\phi^2P + \mathfrak{a}_5\phi P^2 \\ &\quad + \mu P + \mathcal{C}_{\tilde{\beta}}\beta - \mathcal{C}_{\tilde{R}}\dot{\beta} + \mathcal{C}_{\tilde{\delta}_a}\delta_a) \\ &= \mathcal{A}_1\phi + \mathcal{A}_2P + \mathcal{A}_3\phi^2P + \mathcal{A}_4P^3 + \mathcal{A}_5\phi P^2 \\ &\quad + L_\beta\beta - L_R\beta_r + L_{\delta_a}\delta_a \end{aligned} \quad (4)$$

where $\mathcal{A}_1 = a_1/\mathcal{I}_{\mathcal{XX}}$, $\mathcal{A}_2 = (a_2+\mu)/\mathcal{I}_{\mathcal{XX}}$, $\mathcal{A}_3 = a_4/\mathcal{I}_{\mathcal{XX}}$, $\mathcal{A}_4 = a_3/\mathcal{I}_{\mathcal{XX}}$, $\mathcal{A}_5 = a_5/\mathcal{I}_{\mathcal{XX}}$, $L_\beta = \mathcal{C}_{\tilde{\beta}}/\mathcal{I}_{\mathcal{XX}}$, $L_R = \mathcal{C}_{\tilde{R}}/\mathcal{I}_{\mathcal{XX}}$, $L_{\delta_a} = \mathcal{C}_{\tilde{\delta}_a}/\mathcal{I}_{\mathcal{XX}}$. Neglecting the lateral forces due to β, the resulting yaw moment involving the yaw angle $(-\beta)$ and yaw rate $(-\dot{\beta})$ is defined as

$$\mathcal{I}_{\mathcal{ZZ}}\ddot{\beta} = -\mathcal{C}_P P - \mathcal{C}_\beta\beta + \mathcal{C}_R\dot{\beta} \quad (5)$$

where $\mathcal{I}_{\mathcal{ZZ}}$ denotes the moment of inertia about the Z-axis, and $\mathcal{C}_P, \mathcal{C}_\beta$, and $\mathcal{C}_R$ are the coefficients of the roll moment, sideslip angle and yaw moment, respectively. As in (1), after splitting (5), we can extract β and the sideslip angle rate β_r as follows:

$$\dot{\beta} = \beta_r \quad (6)$$

$$\dot{\beta}_r = -N_P P - N_\beta\beta + N_R\beta_r \quad (7)$$

where $N_P = \mathcal{C}_P/\mathcal{I}_{\mathcal{ZZ}}$, $N_\beta = \mathcal{C}_\beta/\mathcal{I}_{\mathcal{ZZ}}$, and $N_R = \mathcal{C}_R/\mathcal{I}_{\mathcal{ZZ}}$. To realize the WRP and cope with the actuation command, the dynamics of an aileron actuator is expressed as:

$$\dot{\delta}_a = \mathcal{T}(\delta_{a^{com}} - \delta_a) + \mathcal{D}_a \quad (8)$$

where δ_a and $\delta_{a^{com}}$ are the aileron deflection and the commanded aileron deflection respectively. The actuator dynamics acts as a control input. $\mathcal{T}$ is the time constant of the actuator and $\mathcal{D}_a$ is the lumped external disturbance.

Remark 2.1: $|\mathcal{D}_a| \leq \mathcal{D}\ \forall\ t \in \Re^{0+}$, where $\mathcal{D}$ is a constant defining the upper bound of external disturbance.

Consider the following general wing rock nonlinear system as:

$$\begin{aligned}\dot{\mathfrak{X}} &= \mathcal{F}(\mathfrak{X}) + \mathcal{BU} + \mathfrak{D} \\ \mathcal{Y} &= \mathcal{H}\mathfrak{X} \\ \mathfrak{X}(0) &= \mathfrak{X}^0 \end{aligned} \quad (9)$$

where

$$\mathcal{F}(\mathfrak{X}) = \begin{bmatrix} P \\ \mathcal{A}_1\phi + \mathcal{A}_2 P + \mathcal{A}_3\phi^2 P + \mathcal{A}_4 P^3 + \cdots \\ \mathcal{A}_5\phi P^2 + L_\beta\beta - L_R\beta_r + L_{\delta_a}\delta_a \\ \beta_r \\ -N_P P - N_\beta\beta + N_R\beta_r \\ -\mathcal{T}\delta_a \end{bmatrix}$$

$$\mathcal{BU} = \begin{bmatrix} 0 \\ 0 \\ 0 \\ 0 \\ \mathcal{T}\delta_{a^{com}} \end{bmatrix}, \quad \mathfrak{D} = \begin{bmatrix} 0 \\ 0 \\ 0 \\ 0 \\ \mathcal{D}_a \end{bmatrix}, \quad \mathcal{H} = \begin{bmatrix} 1 \\ 0 \\ 0 \\ 0 \\ 0 \end{bmatrix}^T$$

Moreover, $\mathfrak{X} = [\,\phi\ P\ \beta\ \beta_r\ \delta_a]^T$ is a state vector, $\mathcal{U}$ is a control input variable, and $\mathcal{Y}$ is the desired output that needs to be controlled or stabilized. So objective of this study is narrated as follows:

Given a desired set point $\mathfrak{X}_\phi^{tg}$, design a feedback control algorithm to suppress the limit cycles that cause the WRP such that $\mathfrak{X}_\phi^{tg}$ is an attractive set for (9) by existing $\mathcal{W} > 0$, such that, $\mathfrak{X}(t : t_0, \mathfrak{X}^0) \to \mathfrak{X}_\phi^{tg}$ as $t \to \infty$ for any initial condition $(t_0, \mathfrak{X}^0) \in \Re^+ \times \mathcal{P}(\mathfrak{X}_\phi^{tg} : \mathcal{W})$. For the synthesis of the control objectives, the following assumption is made

Assumption 2.2: Wing Rock's nonlinear model is controllable and output controllable.

3. Controller design

In this section, the PI-based low-order observer and second-order sliding mode control scheme are discussed.

3.1. Observer design

The availability of system states is crucial for system monitoring, control and stabilization. However not all the states can be directly measured in general. Therefore, the measured output is used to estimate the unknown state. State estimation depends on observability. If this condition is fulfilled, it means that the state can be estimated. If, at any initial condition, a state vector can be extracted from the output of the system in finite time, then the system is observable. To verify the observability of the nonlinear dynamical systems, an observation space (Boutat & Zheng, 2021) is established as follows:

$$\mathcal{O} = \begin{bmatrix} \mathcal{Y} \\ \dot{\mathcal{Y}} \\ \ddot{\mathcal{Y}} \\ \vdots \\ \mathcal{Y}^{\mathrm{j}} \end{bmatrix} = \begin{bmatrix} \mathcal{H} \\ L_{\mathcal{F}}\mathcal{H} \\ L_{\mathcal{F}}^2\mathcal{H} \\ \vdots \\ L_{\mathcal{F}}^{\mathrm{j}}\mathcal{H} \end{bmatrix} \tag{10}$$

where $\mathcal{F} \in \mathcal{C}^\infty$ and $\mathcal{H} \in \mathcal{C}^\infty$, $\mathcal{Y}^{\mathrm{j}}$ is the kth time derivative of $\mathcal{Y}$, $L_{\mathcal{F}}^{\mathrm{j}}\mathcal{H}$ is the kth Lie derivative of $\mathcal{H}$ in the direction of $\mathcal{F}$. If the observation space satisfies condition (11), then the nonlinear dynamical system is observable in the local ($x \in X$) or global ($x \in \Re^n$) context.

$$\dim\left(\mathrm{d}\mathcal{O}|_x\right) = \mathcal{N} \tag{11}$$

where $\mathcal{N}$ is the rank number and the proposed observer is modelled as

$$\begin{aligned} \dot{X} &= F(X) + \mathcal{K}_{\mathcal{S}} X^* \\ \dot{\hat{X}} &= F(X) + \measuredangle_{\mathcal{I}}^{\mathcal{P}} \end{aligned} \tag{12}$$

where $F(X)$ is a nonlinear function of the known states of the system, $\mathcal{K}_{\mathcal{S}} \in \Re$ and X^* is unknown state. $\measuredangle_{\mathcal{I}}^{\mathcal{P}}$ is PI term and can be represented as

$$\begin{aligned} \measuredangle_{\mathcal{I}}^{\mathcal{P}} &= \mathcal{K}_{\mathcal{P}}^o E + \bar{\mathcal{K}}_{\mathcal{I}}^o \mathcal{I}^o \\ \dot{\mathcal{I}}^o &= \mathcal{K}_{\mathcal{I}}^o E \\ E &= \frac{2}{\pi}\tan^{-1}(\bar{\Delta}\tilde{X}) \end{aligned} \tag{13}$$

where $\mathcal{K}_{\mathcal{P}}^o \in \Re$, $\mathcal{K}_{\mathcal{I}}^o \in \Re$, and $\bar{\mathcal{K}}_{\mathcal{I}}^o \in \Re$ are proportional, integral and distributive gains respectively. It can be realized from (13) that E is the output error and must quickly converge to zero. To accomplish this, a convergence function with $\bar{\Delta} \in \Re^+$ is implemented, where $\bar{\Delta}$ serves as the convergence speed constant. According to $\tilde{X} = X - \hat{X}$, the following relationship can be obtained as:

$$\dot{\tilde{X}} = \mathcal{K}_{\mathcal{S}} X^* - \measuredangle_{\mathcal{I}}^{\mathcal{P}} \tag{14}$$

By imposing $\measuredangle_{\mathcal{I}}^{\mathcal{P}}$ on error $\tilde{X} = X - \hat{X}$, it is possible to estimate the unknown state X^*. The convergence of $\tilde{X}$ can be established by assigning the gains of $\measuredangle_{\mathcal{I}}^{\mathcal{P}}$ such that $E \to 0$ and $\mathcal{I}^o \to 0$ as $t \to \infty$. Based on an equivalent control concept (V.I. Utkin, 2013), substituting $\tilde{X} = \dot{\tilde{X}} = 0$, the equivalent value of (14) can be found as

$$\hat{X}^* = \frac{(\measuredangle_{\mathcal{I}}^{\mathcal{P}})_{eq}}{\mathcal{K}_{\mathcal{S}}} \tag{15}$$

Remark 3.1: It is observed that after adding the convergence function, the gains of $\measuredangle_{\mathcal{I}}^{\mathcal{P}}$ need to be chosen less than the corresponding gains without the convergence function, and the proportional term is also responsible for the convergence error while the integral term reduces the steady-state error.

In this study, the unknown state β can be estimated by compelling $\measuredangle_{\tilde{\mathcal{P}}}$ term on the error $\tilde{P}$ as

$$\dot{\hat{P}} = \mathcal{A}^{\mathcal{A}} + \mathcal{B}^{\mathcal{B}} + \measuredangle_{\tilde{\mathcal{P}}}$$
$$\dot{\tilde{P}} = L_\beta \beta - \measuredangle_{\tilde{\mathcal{P}}} \tag{16}$$

where $\mathcal{A}^{\mathcal{A}} = \mathcal{A}_1\phi + \mathcal{A}_2 P + \mathcal{A}_3\phi^2 P + \mathcal{A}_4 P^3 + \mathcal{A}_5\phi P^2$, $\mathcal{B}^{\mathcal{B}} = L_{\delta_a}\delta_a - L_R\beta_r$. After employing equivalent control approach, β can be estimated as

$$\hat{\beta} = \frac{(\measuredangle_{\tilde{\mathcal{P}}})_{eq}}{L_\beta} \tag{17}$$

3.2. Second order sliding mode control

In first order Sliding Mode Control (FOSMC), the equivalent control (U_{eq}) is formulated by calculating the first derivative of the sliding manifold $\mathcal{S}_{\mathcal{M}}$ and obeys the essential stability requirement ($\mathcal{S}_{\mathcal{M}}\dot{\mathcal{S}}_{\mathcal{M}} < 0$) (Mahmood & Bhatti, 2023; Mahmood, Okasha & Saeed, 2024; Mahmood, 2025; V. Utkin, Poznyak, Y.V. Orlov et al., 2020). The FOSMC's key challenge is to ensure the reaching phase in terms of state or error, and then to ensure sliding motion at the specified sliding manifold $\mathcal{S}_{\mathcal{M}}$ (Mechali et al., 2022; Ullah et al., 2016). Another situation exists in which U_{eq} arises after considering multiple time derivatives of $\mathcal{S}_{\mathcal{M}}$. This approach is called the rth SMC if $\mathcal{S}_{\mathcal{M}} = \dot{\mathcal{S}}_{\mathcal{M}} = \ddot{\mathcal{S}}_{\mathcal{M}} = \cdots = \mathcal{S}_{\mathcal{M}}^{n-1} = 0$. In the rth SMC, the main intention is to steer the state or error on the sliding manifold $\mathcal{S}_{\mathcal{M}}$ and ensure its successive derivatives to zero (V. Utkin, Poznyak, Y. Orlov et al., 2020). In the case of SOSMC, the control law aims to drive the sliding manifold $\mathcal{S}_{\mathcal{M}}$ and its derivative $\dot{\mathcal{S}}_{\mathcal{M}}$ to null (Ding et al., 2021).

Remark 3.2: rth SMC also deals with affine systems. The design procedures of the FOSMC and SOSMC are similar and consist of consecutive selection of a $\mathcal{S}_{\mathcal{M}}$. The control law enforces state trajectories to this manifold.

3.2.1. Nonlinear second order sliding mode control

To dampen the WRP, the difference between the referenced roll angle ϕ_d and the actual roll angle ϕ is treated as a control variable in the SOMSC, and the controller formulates a control input that is applied to the wing rock dynamic model to achieve the desired objective. The tracking error is defined as follows:

$$\mathcal{E} = \phi - \phi_d \tag{18}$$

Based on (18), the three consecutive derivatives of the tracking error dynamics are given as

$$\begin{cases} \dot{\mathcal{E}} = P - \dot{\phi}_d \\ \ddot{\mathcal{E}} = \dot{P} - \ddot{\phi}_d \\ \dddot{\mathcal{E}} = \Im + \wp\dot{P} + \eth\delta_{a_{com}} + L_{\delta_a}\mathcal{D}_a - \dddot{\phi}_d \end{cases} \tag{19}$$

where $\Im = \mathcal{A}_1 P + 2\mathcal{A}_3\phi P^2 + \mathcal{A}_5 P^3 + L_\beta\beta_r + L_R(N_P P + N_\beta\hat{\beta} - N_R\beta_r) - \eth\delta_a$, $\wp = \dot{P}(\mathcal{A}_2 + 3\mathcal{A}_4 P^2 + \mathcal{A}_3\phi^2 + 2\mathcal{A}_5\phi P)$, and $\eth = \mathcal{T}L_{\delta_a}$. The expected performance of the SMC is determined by the planned sliding manifold (Afifa et al., 2023). To address the trade-off between effectiveness and control effort while achieving convergence behaviour and improved transient response, the following nonlinear sliding manifold is developed:

$$\mathcal{S}_{\mathcal{M}} = \Gamma \tanh(\mathcal{E}) + \Upsilon\dot{\mathcal{E}} \tag{20}$$

where $\Gamma, \Upsilon \in \Re^+ > 0$. To satisfy the convergence of the error on the sliding manifold $\mathcal{S}_{\mathcal{M}}$, a Lyapunov function $\mathcal{V} = 0.5\mathcal{E}^2$ is considered. The reduced-order dynamics can be formulated to attain error convergence as follows:

$$\dot{\mathcal{V}} = \mathcal{E}\dot{\mathcal{E}} = -\Gamma\Upsilon^{-1}\mathcal{E}\tanh(\mathcal{E}) \tag{21}$$

Eventually, the tracking error will converge to $\mathcal{S}_{\mathcal{M}}$ by selection of proper design gains Γ, Υ. The time required to converge any initial error $\mathcal{E}(t_0)$ to the equilibrium error $\mathcal{E}(t_e)$ is computed as

$$t_c = \Upsilon(\ln(\sinh(\mathcal{E}(t_0)) - \ln(\sinh(\mathcal{E}(t_e)))/\Gamma \tag{22}$$

Remark 3.3: The derivative of *tanh* may increase the complexity of overall control law but has a positive effect as it increases the error convergence rate and eliminates the undershoot/overshoot because it is smooth, uniformly bounded, monotonic, antisymmetric and has convexity for $\Re^-$ while concavity for $\Re^+$.

To design the SOSMC, two successive derivatives of the desired $\mathcal{S}_{\mathcal{M}}$ are taken as

$$\begin{cases} \dot{\mathcal{S}}_{\mathcal{M}} = \Gamma\varnothing\dot{\mathcal{E}} + \Upsilon\ddot{\mathcal{E}} \\ \ddot{\mathcal{S}}_{\mathcal{M}} = \Gamma\varnothing(\ddot{\mathcal{E}} - 2\dot{\mathcal{E}}^2\tanh\mathcal{E}) + \Upsilon\dddot{\mathcal{E}} \end{cases} \tag{23}$$

where $\varnothing = 1/\cosh^2(\mathcal{E})$. The equivalent control ($\mathcal{U}_{\text{eq}}$) acts as a continuous control during contact with the sliding manifold and ensures that the change in the system trajectory of the system is perpendicular to the sliding manifold $\mathcal{S}_{\mathcal{M}}$. Thus, $\mathcal{U}_{eq}$ of SOSMC offers asymptotic convergence of the $\mathcal{S}_{\mathcal{M}}$ to zero according to the desired problem. To maintain the trajectories on $\mathcal{S}_{\mathcal{M}}$ while developing the SMC, $\mathcal{U}_{\text{eq}}$ is first established. According to the equivalent control principle $\ddot{\mathcal{S}}_{\mathcal{M}} = 0$, we obtain

$$\mathcal{U}_{\text{eq}} = \Gamma\varnothing(2\dot{\mathcal{E}}^2\tanh\mathcal{E} - \ddot{\mathcal{E}})/\Upsilon\eth + (\dddot{\phi}_d - \Im - \wp\dot{P})/\eth \tag{24}$$

To ensure finite time convergence and the sliding motion of the system trajectory on $\mathcal{S}_{\mathcal{M}}$, a discontinue control ($\mathcal{U}_{\text{dis}}$) having high-frequency switching control is introduced which makes the SMC law insensitive to disturbances and uncertainties (Ajwad et al., 2015). Owing to

high-frequency switching, chattering is introduced which degrades the performance of the SMC and may saturate the actuators. To cope with this inherent problem in SMC, discontinuous control ($\mathcal{U}_{\text{dis}}$) is introduced as:

$$\mathcal{U}_{\text{dis}} = -\frac{2}{\pi}\bar{\mathcal{K}}\tan^{-1}(\beth\dot{\mathcal{S}}_{\mathcal{M}}) - \frac{2}{\pi}\tilde{\mathcal{K}}\tan^{-1}(\gimel\mathcal{S}_{\mathcal{M}}) \quad (25)$$

where $\bar{\mathcal{K}}$, $\tilde{\mathcal{K}} \in \Re^{+}$ are switching gains, and $\beth$, $\gimel \in \Re^{+}$ tune the convergence speed by adjusting the slope of the switching function defined as

$$\frac{2}{\pi}\tan^{-1}(\mathcal{S}_{\mathcal{M}}) = \begin{cases} 1, & \mathcal{S}_{\mathcal{M}} > 0 \\ 0, & \mathcal{S}_{\mathcal{M}} = 0 \\ -1, & \mathcal{S}_{\mathcal{M}} < 0 \end{cases} \quad (26)$$

To achieve suppression of wing rock and robustness against disturbances, the SOSMC law ($\mathcal{U}_{\delta_a\text{com}} = \mathcal{U}_{\text{eq}} + \mathcal{U}_{\text{dis}}$) is designed as follows:

$$\mathcal{U}_{\delta_a\text{com}} = \Gamma\varnothing(2\dot{\mathcal{E}}^2\tanh\mathcal{E} - \ddot{\mathcal{E}})/\Upsilon\eth + (\dddot{\phi}_d - \Im - \wp\dot{P})/\eth - \frac{2}{\pi}\bar{\mathcal{K}}\tan^{-1}(\beth\dot{\mathcal{S}}_{\mathcal{M}}) - \frac{2}{\pi}\tilde{\mathcal{K}}\tan^{-1}(\gimel\mathcal{S}_{\mathcal{M}}) \quad (27)$$

After developing the proposed SOSMC for wing rock, the closed-loop existence of the SOSMC can be corroborated by the following theorem.

Theorem 3.1: *The closed-loop existence of the SOSMC law for the wing rock dynamic model* (9) *can be globally asymptotically stable in the presence of the proposed sliding manifold* $\mathcal{S}_{\mathcal{M}}$ (20) *and the proposed embedded law* $\mathcal{U}_{\delta_a com}$ (27) *if the discontinuous control gains* $\tilde{\mathcal{K}}$ *and* $\bar{\mathcal{K}}$ *satisfy the following conditions:*

$$\bar{\mathcal{K}} > \mathcal{D}, \quad \bar{\mathcal{K}} \in \Re^{+}$$
$$\tilde{\mathcal{K}} > 1/\Upsilon\eth, \quad \tilde{\mathcal{K}} \in \Re^{+} \quad (28)$$

Consequently, ϕ *will converge to the set point to eliminate the WRP.*

Proof: To demonstrate the existence claim of SOSMC and confirm the statement of the above theorem, a Lyapunov function (Furat & Eker, 2014) is written as

$$\mathcal{L} = |\mathcal{S}_{\mathcal{M}}| + 0.5\dot{\mathcal{S}}_{\mathcal{M}}^2 \quad (29)$$

Taking the time derivative of $\mathcal{L}$ and then inserting (23) and control law (27) into the resulting equation, we get

$$\begin{aligned}
\dot{\mathcal{L}} &= \frac{|\mathcal{S}_{\mathcal{M}}|}{\mathcal{S}_{\mathcal{M}}}\dot{\mathcal{S}}_{\mathcal{M}} + \dot{\mathcal{S}}_{\mathcal{M}}\ddot{\mathcal{S}}_{\mathcal{M}} \\
&= \frac{|\mathcal{S}_{\mathcal{M}}|}{\mathcal{S}_{\mathcal{M}}}\dot{\mathcal{S}}_{\mathcal{M}} + \dot{\mathcal{S}}_{\mathcal{M}}\left(-\frac{2}{\pi}\Upsilon\eth\bar{\mathcal{K}}\tan^{-1}(\beth\dot{\mathcal{S}}_{\mathcal{M}}) - \frac{2}{\pi}\Upsilon\eth\tilde{\mathcal{K}}\tan^{-1}(\gimel\mathcal{S}_{\mathcal{M}}) + \Upsilon\eth\mathcal{D}_a\right) \\
&\leq \frac{|\mathcal{S}_{\mathcal{M}}|}{\mathcal{S}_{\mathcal{M}}}\dot{\mathcal{S}}_{\mathcal{M}} - \frac{2}{\pi}\Upsilon\eth\tilde{\mathcal{K}}\tan^{-1}(\gimel\mathcal{S}_{\mathcal{M}})\dot{\mathcal{S}}_{\mathcal{M}} + \Upsilon\eth\mathcal{D}_a\dot{\mathcal{S}}_{\mathcal{M}} - \Upsilon\eth\bar{\mathcal{K}}|\dot{\mathcal{S}}_{\mathcal{M}}| \\
&\leq |\dot{\mathcal{S}}_{\mathcal{M}}|\left(\frac{|\mathcal{S}_{\mathcal{M}}|}{\mathcal{S}_{\mathcal{M}}} - \frac{2}{\pi}\Upsilon\eth\tilde{\mathcal{K}}\tan^{-1} \times (\gimel\mathcal{S}_{\mathcal{M}}) + \Upsilon\eth\mathcal{D}_a - \Upsilon\eth\bar{\mathcal{K}}\right) \\
&\leq |\dot{\mathcal{S}}_{\mathcal{M}}|\left(\frac{|\mathcal{S}_{\mathcal{M}}|}{\mathcal{S}_{\mathcal{M}}} - \Upsilon\eth\tilde{\mathcal{K}}\frac{|\mathcal{S}_{\mathcal{M}}|}{\mathcal{S}_{\mathcal{M}}} + \Upsilon\eth(\mathcal{D}_a - \bar{\mathcal{K}})\right) \\
&\leq |\dot{\mathcal{S}}_{\mathcal{M}}|\left(\frac{|\mathcal{S}_{\mathcal{M}}|}{\mathcal{S}_{\mathcal{M}}} - \Upsilon\eth\tilde{\mathcal{K}}\frac{|\mathcal{S}_{\mathcal{M}}|}{\mathcal{S}_{\mathcal{M}}} - \Upsilon\eth(\bar{\mathcal{K}} - \mathcal{D}_a)\right) \\
&\leq |\dot{\mathcal{S}}_{\mathcal{M}}|\left(\frac{|\mathcal{S}_{\mathcal{M}}|}{\mathcal{S}_{\mathcal{M}}}(1 - \Upsilon\eth\tilde{\mathcal{K}}) - \Upsilon\eth(\bar{\mathcal{K}} - \mathcal{D}_a)\right) \quad (30)
\end{aligned}$$

To maintain the negative definiteness of (30), the last inequality provides clear evidence for achieving global asymptotic stability. If we choose $\bar{\mathcal{K}} > \mathcal{D}$, then robustness is ensured against external bounded disturbances and if $\tilde{\mathcal{K}} > 1/\Upsilon\eth$, then sliding motion is guaranteed. Therefore, it can be concluded that the existence of the proposed SOSMC meets the requirements of the theorem. ■

Figure 3 shows a comprehensive block diagram that includes the proposed observer and the controller.

4. Results and discussion

To examine the superiority of the proposed nonlinear SOSMC approach over the classical SOSMC and PID SOSMC, wing rock suppression simulations are illustrated graphically with the proposed observer in the presence of disturbances and without disturbances. Aero coefficients for the WRP simulation of a slender delta-wing aircraft at a 25 deg angle of attack are taken from Zribi et al. (2013). To attain the desired response of wing rock motion, a set point is chosen as $\phi_d = 0$. Moreover, the proposed ROFPI observer gains $\mathcal{K}_{\mathcal{P}}^{o}$, $\mathcal{K}_{\mathcal{I}}^{o}$, and $\bar{\mathcal{K}}_{\mathcal{I}}^{o}$ are selected as 7, 3, 5 and $\bar{\Delta}$ is 7.7 respectively.

4.1. Nominal environment

In this section, an environment without external disturbance is considered and the outcomes of the wing rock

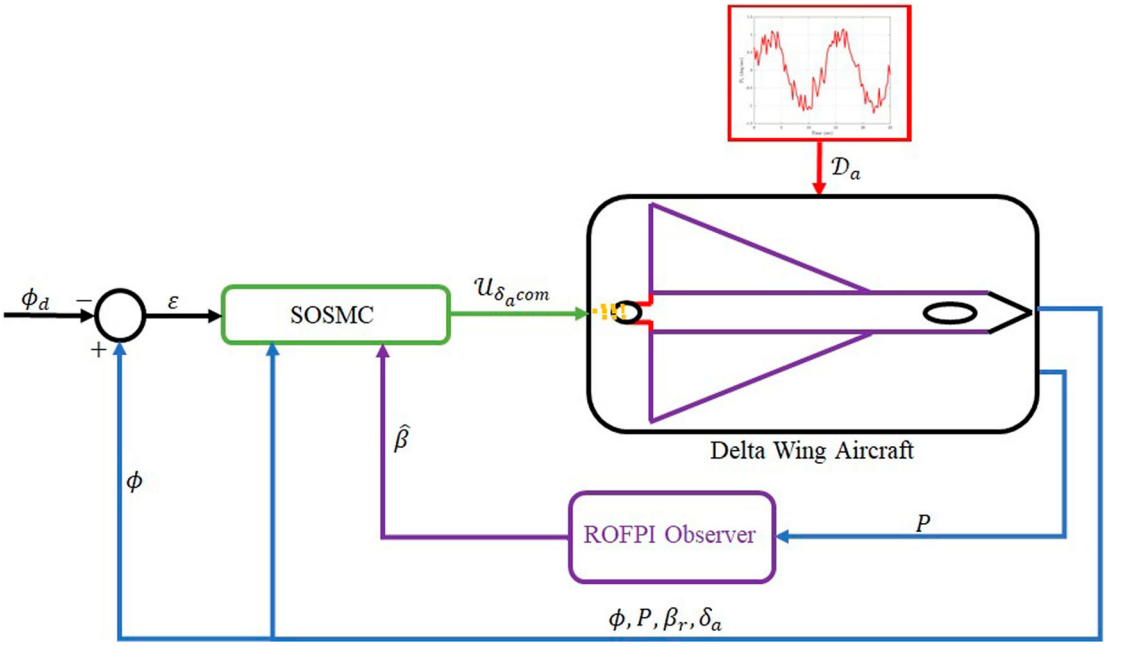

Figure 3. ROFPI observer based SOSMC.

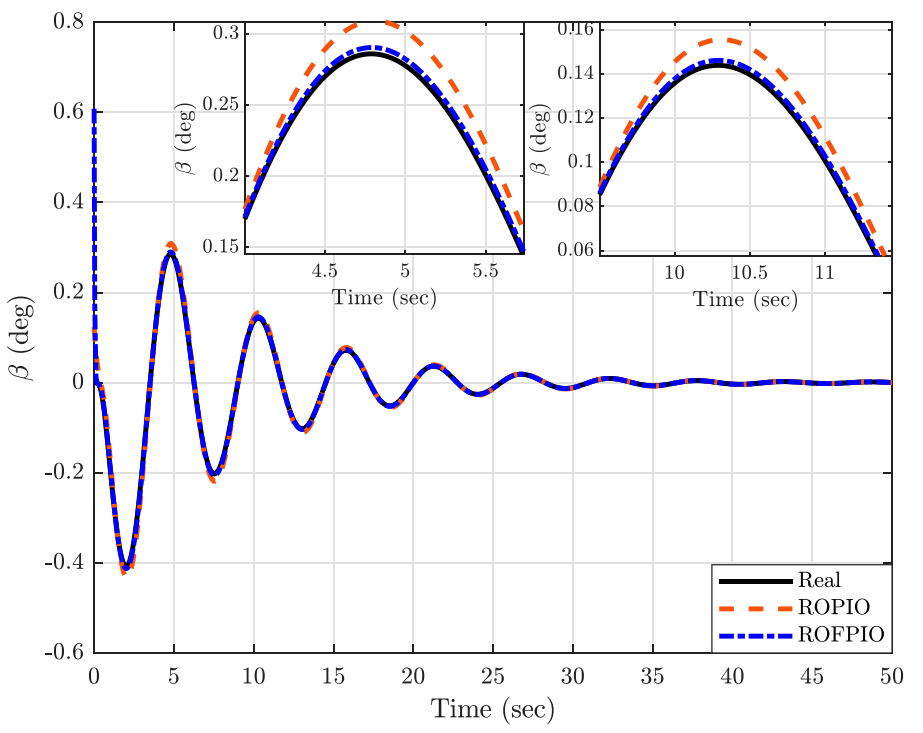

Figure 4. Estimated side slip angle profile.

regulation or stabilization are presented. To approximate the side slip angle of the wing rock dynamic model, a comparative analysis between the ROPI and ROFPI observers is shown in Figure 4, where it can be noted that the ROFPI observer is outperforming the ROPI observer in terms of convergence. Additionally, in terms of estimation error, Figure 5 evaluate the effectiveness of the suggested observer. It is vital to remember that the observer gains $\mathcal{K}_{\mathcal{P}}^{o}$, $\mathcal{K}_{\mathcal{I}}^{o}$ and $\bar{\mathcal{K}}_{\mathcal{I}}^{o}$ are kept same for both observers.

It is important to point out that the discontinuous control $\mathcal{U}_{\text{dis}}$ is kept the same for both the referenced control approaches and the nonlinear SOSMC approach by choosing the gains as $\bar{\mathcal{K}} = 2$, $\tilde{\mathcal{K}} = 5$, $\beth = 3$ and $\gimel = 1$ respectively. The set point tracking of the roll angle ϕ

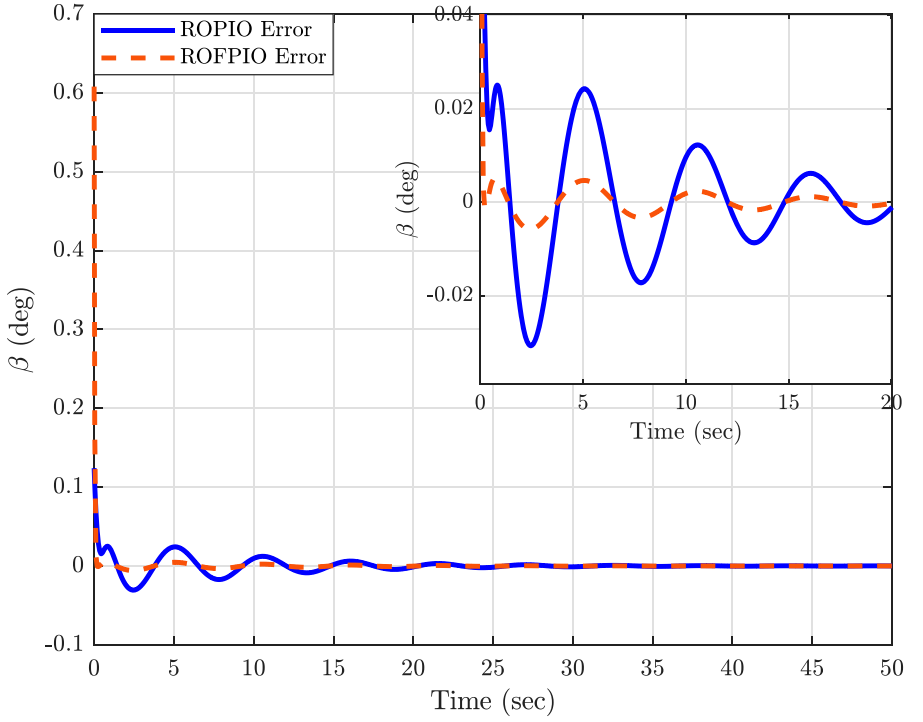

Figure 5. Estimation error profile.

in the presence of the proposed SOSMC is illustrated in Figure 6. The proposed control approach publicizes the desired roll angle in terms of settling time with a negative overshoot. Classical SOSMC and PID SOSMC stabilize the roll angle within 6.02 sec and 6.31 sec respectively. Furthermore, the suggested *tanh* SOSMC nullifies the WRP within 4.61 sec. Compared with classical SOSMC and PID SOSMC control algorithms, the proposed SOSMC has zero negative overshoot.

Figure 7 presents the results of the roll rate and it can be identified that the proposed and classical controllers demonstrate stable performance. In contrast, the PID SOSMC controller delivers a jerky response, leading to a negative overshoot during the stabilization of the roll angle. In Figure 8, phase portrait is illustrated as a way to analyse the dynamic behaviour of the controllers under investigation. The controllers asymptotic stability and phase trajectory towards the equilibrium point are evident from the figure. The wing rock model's convergence can also be seen in the phase portrait and it is clear that the proposed controller's phase trajectory has a faster response than the classical SOSMC and PID SOSMC controllers.

The deflection response of the aileron is illustrated in Figure 9 which also manifests the requirement on the aileron to stabilize the wing rock dynamics. Therefore, it is evident that the proposed controller generates a lower burden on the control surfaces and converges the ϕ in less settling time with negligible negative overshoot. The proposed SOSMC controller yields -10 deg to 8.8 deg less deflection, and then the aileron becomes stable after 4.5 sec. It is vital to the highlight that same design gains in the discontinuous control for all the three controllers are considered in order to fairly investigate the suppression response of wing rock.

To evaluate the performance of the stated controllers, a numerical observation is made in terms of average power (P_{avg}) and integral absolute value (IAV). The average power represents the energy consumed by the given controllers, whereas IAV indicates the load on the aileron control surface caused by the provided controllers. P_{avg} and IAV are given by (31) and (32) respectively.

$$P_{\text{avg}}^{\mathcal{U}} = \frac{1}{\aleph}\sum_{\mathcal{I}=1}^{\aleph}(\mathcal{U}_{\delta_{a\text{com}}}(\mathcal{I}))^2 \tag{31}$$

$$\delta_a^{\text{IAV}} = \int_{t_0}^{t_f} |\delta_a|\,\mathrm{d}t \tag{32}$$

where $\aleph$ indicates the number of total time samples. Table 1 presents the performance indices and from table, the numerical statistics indicates that the proposed controller consumes 28.67% less power than the classical SOSMC and 19.41% less power than the PID SOSMC. Furthermore, compared with the classical SOSMC, the proposed controller also exerts 7.33% less stress on the aileron control surfaces, and compared with the PID

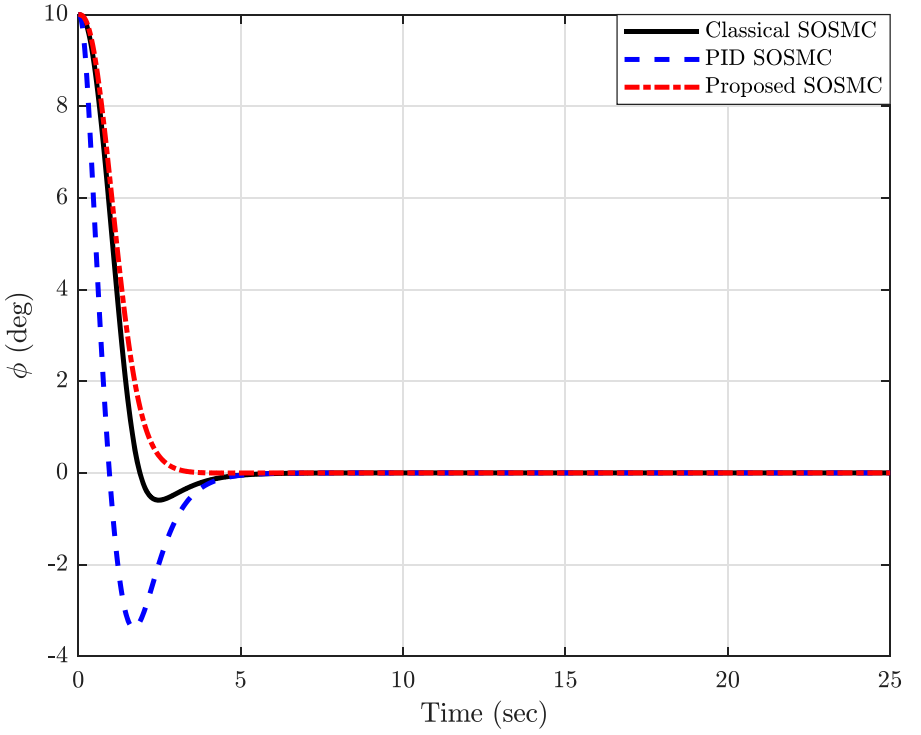

Figure 6. Roll angle.

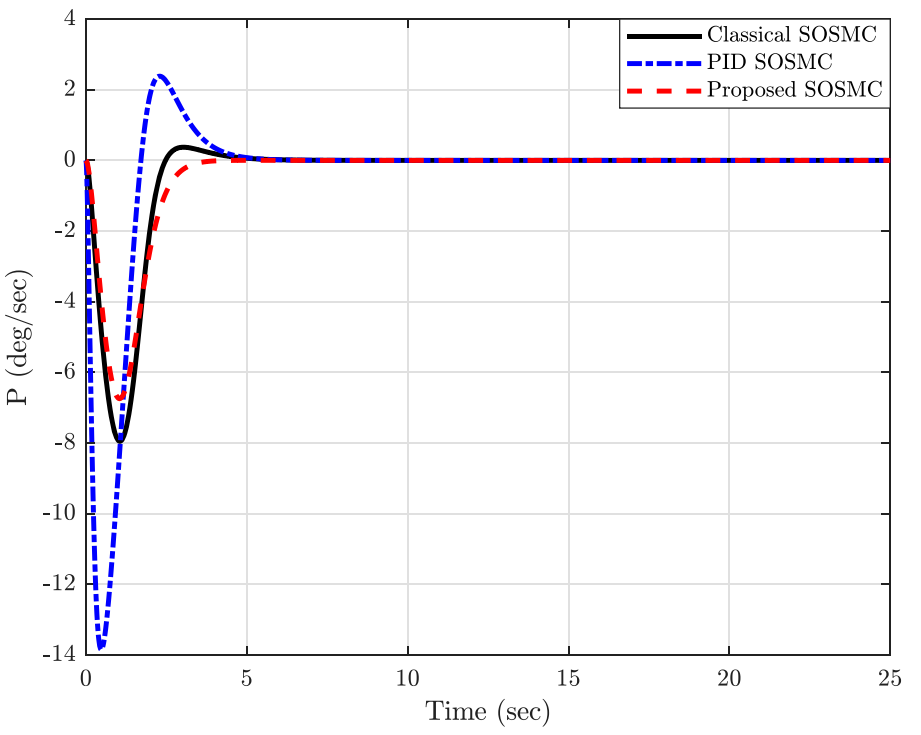

Figure 7. Roll rate.

SOSMC, it experiences 16.29% less aileron stress. Consequently, the nonlinear sliding manifold-based SOSMC for the wing rock dynamic model achieves zero negative overshoot and superior control performance with low average power and load on the aileron control surface.

4.2. Disturbed environment

In this section, the performance of the proposed SOSMC subject to an external disturbance $\mathcal{D}_a$ is analysed and compared with other SOSMC-based controllers. For this

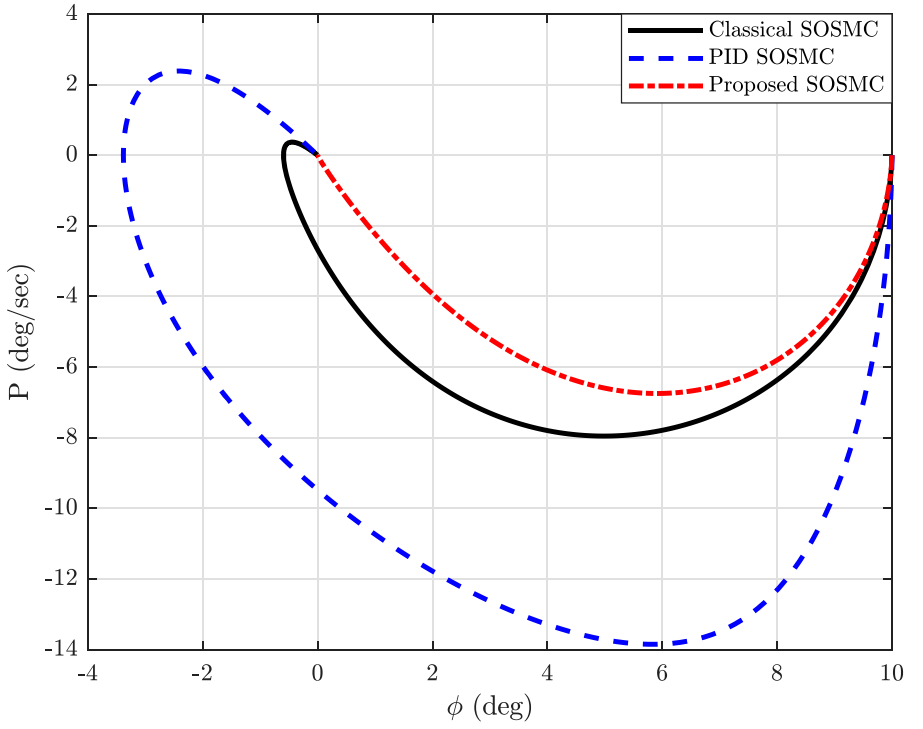

Figure 8. Phase portrait.

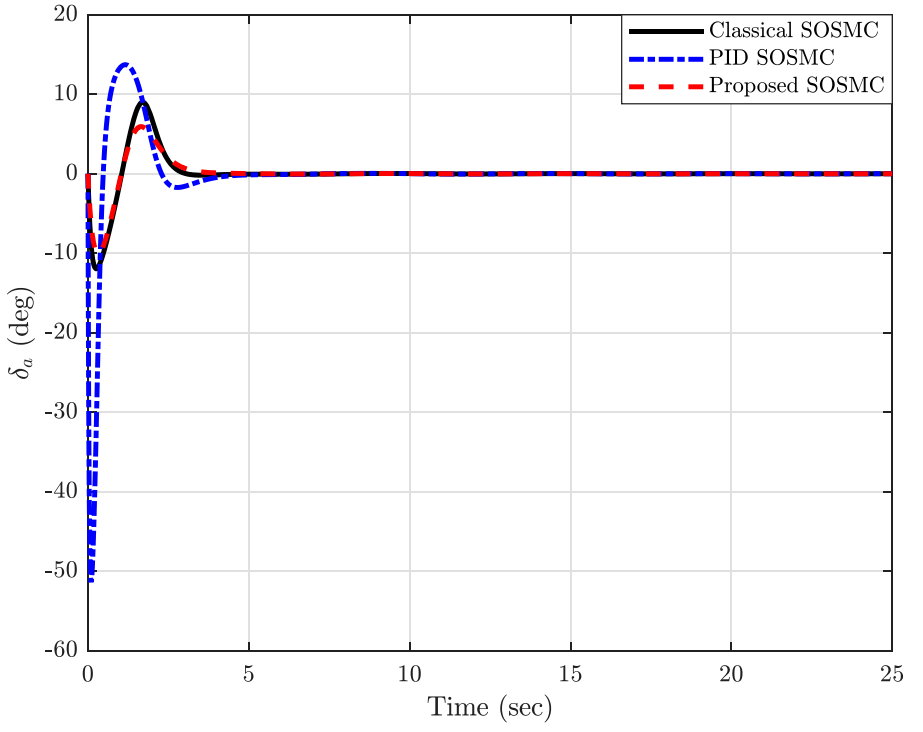

Figure 9. Aileron deflection.

purpose, a white Gaussian noise-based sinusoidal disturbance $\mathcal{D}_a$ (deg/sec) is inoculated in (8), and is illustrated in Figure 10. In the presence of $\mathcal{D}_a$, the gains of discontinuous control for the aforementioned control schemes are given as $\bar{\mathcal{K}} = 2.3$, $\tilde{\mathcal{K}} = 2$, $\beth = 30$ and $\daleth = 25$, respectively.

Table 1. Performance indices.

Controller	P_{avg} (rad/sec)^2	IAV (rad)
Classical SOSMC	5.8196	16.6621
PID SOSMC	36.0300	32.6202
Proposed SOSMC	3.2701	13.6787

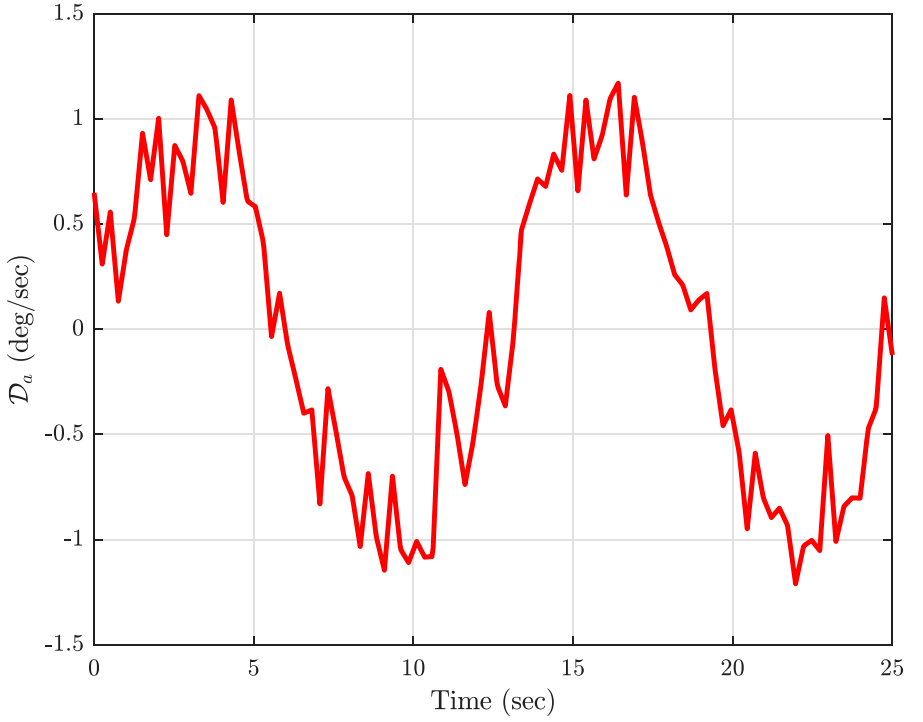

Figure 10. White Gaussian disturbance.

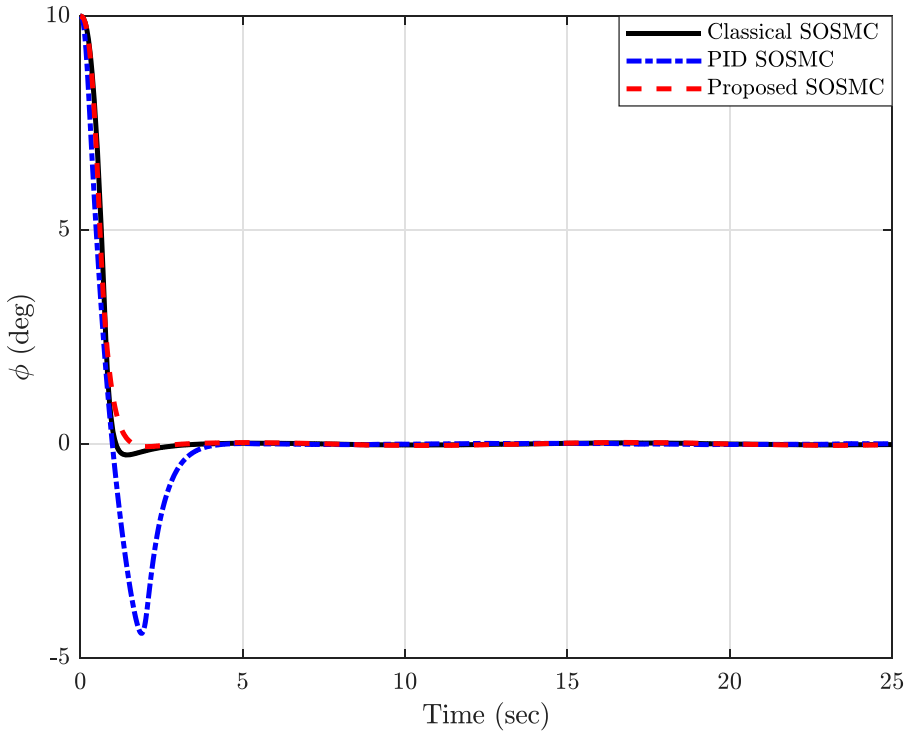

Figure 11. Roll angle profile.

Roll angle simulations in the presence of disturbances are shown in Figure 11 and it can be investigated that the proposed controller demonstrates robustness similar to classical SOSMC and PID SOSMC with zero negative overshoot. Conversely, a negative overshoot in classical and PID SOSMC controllers results in a degradation of the controller's performance. The proposed method synthesizes the settling time for the roll angle in 3.6 sec, while the classical and PID SOSMC controllers require 4.4 sec and 5.4 sec respectively.

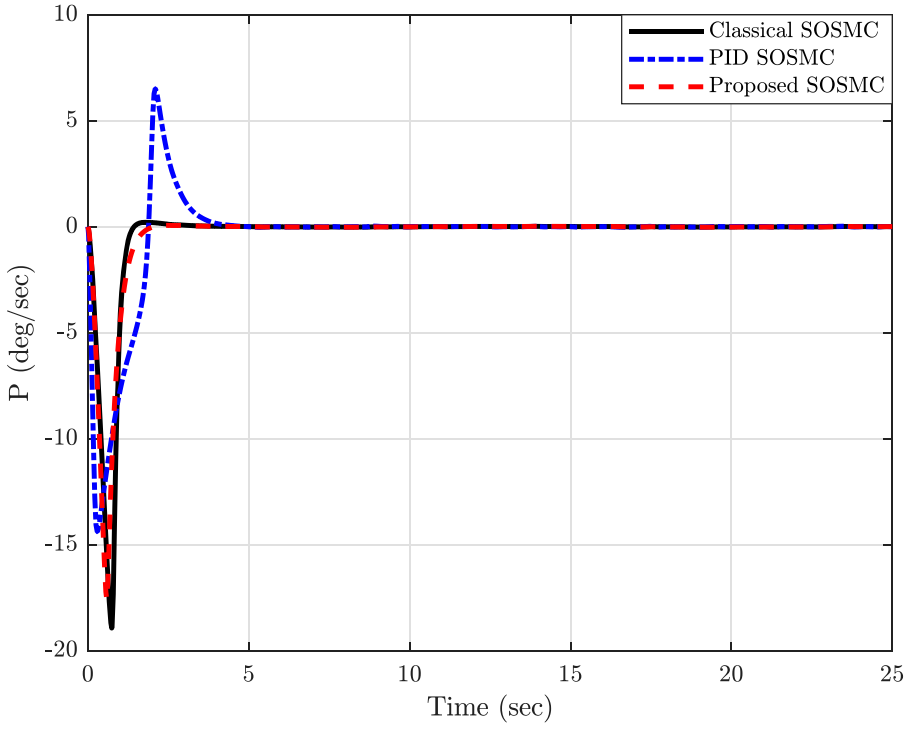

Figure 12. Roll rate profile.

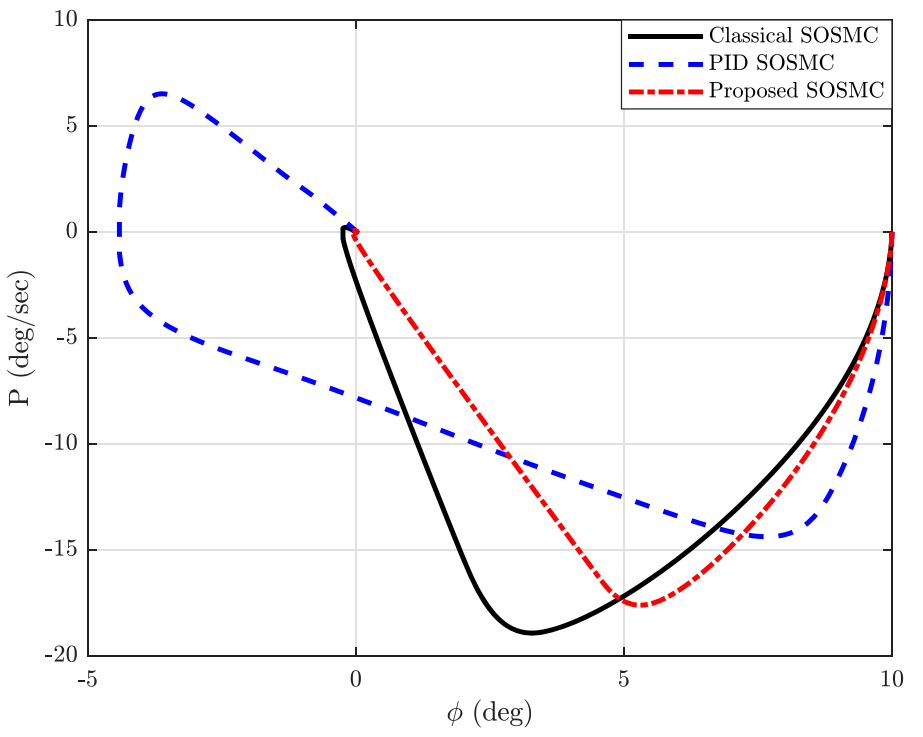

Figure 13. Phase portrait.

According to the roll rate results in Figure 12, the proposed controller produces a roll rate of −17 deg/sec. while the classical SOSMC controller produces a roll rate of −19.4 deg/sec. The PID SOSMC shows an undesirable roll rate response with a minimum of −14.8 deg/sec and a maximum of 6.2 deg/sec, resulting in a very slow settling time of 4.4 sec when compared to classical and proposed SOSMC laws. As opposed to the proposed and PID SOSMC controllers, the classical SOSMC controller stabilizes the roll rate quickly. The controllers behaviour against the

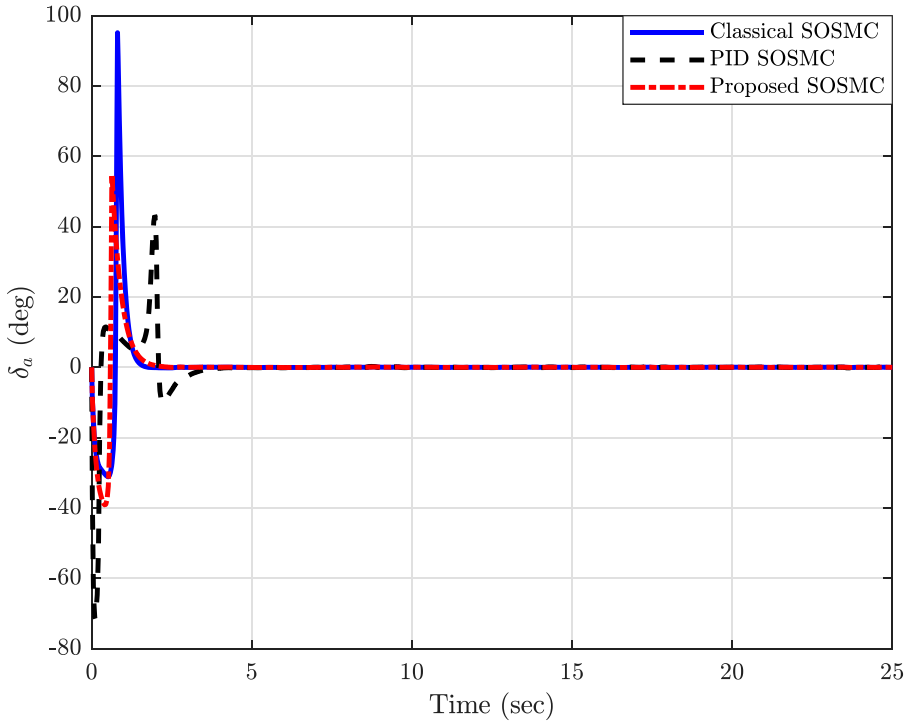

Figure 14. Aileron deflection profile.

disturbance in order to inhibit wing rock motion is illustrated by the phase portrait given in Figure 13. The classical SOSMC and PID SOSMC produce phase trajectories at a slower rate than the proposed controller, which attracts the phase trajectory towards the equilibrium point after a −17 deg/sec roll rate variation.

To devastate the external disturbance, the SOSMC induces a high-amplitude control law to actuate a first-order actuator that responds in aileron deflection. Figure 14 depicts the aileron deflection profile in the presence of disturbance. The classical controller demonstrates a high deflection profile with a maximum deflection of 98.2 deg, and the PID SOSMC controller also produces a high deflection of 42 deg to mitigate the disturbance and wing rock motion. However, in comparison to the aileron deflection demonstrated by the classical SOSMC and PID SOSMC, the proposed controller delivers less deflection and stress on the aileron control surfaces, resulting in stable response with zero negative overshoot.

Numerical results of energy dissipation and load on the aileron control surface in the presence of disturbance are presented in Table 2. Based on the numerical data, the proposed controller effectively reduces disturbances with 28.67% less power compared to the classical SOSMC and 19.41% less power compared to PID SOSMC. Additionally, the proposed controller also experiences 7.33% less aileron stress compared to the classical SOSMC and 16.29% less aileron stress compared to the PID SOSMC.

Table 2. Performance indices in the presence of disturbance.

Controller	P_{avg} (rad/sec)^2	IAV (rad)
Classical SOSMC	82.4874	38.5097
PID SOSMC	73.0062	42.6337
Proposed SOSMC	58.8346	35.6888

4.3. Monte Carlo simulations

The effectiveness of the proposed control strategy is further evaluated using Monte Carlo based simulations. The primary aim is to demonstrate the robustness of the designed control law considering various parameters such as; time period, amplitude and signal-to-noise ratio (SNR) of the sinusoidal white Gaussian external disturbance as illustrated in Figure 10. It is pertinent to mention that the discontinuous control ($\mathcal{U}_{dis}$) remains consistent with the one used in the disturbed environment. A total of 1000 simulations are conducted, each focusing on the time period, amplitude and SNR of the external disturbance.

Figure 15 illustrates the simulations corresponding to the time period ranging from 0.5 sec to 5 sec. The average settling time is approximately 4 sec, which is comparable to the settling time obtained by the proposed controller in case of a disturbed environment. Furthermore, the zoomed portion of the Figure 15 highlights that the time period has a significant effect on the steady-state response of the roll angle ϕ.

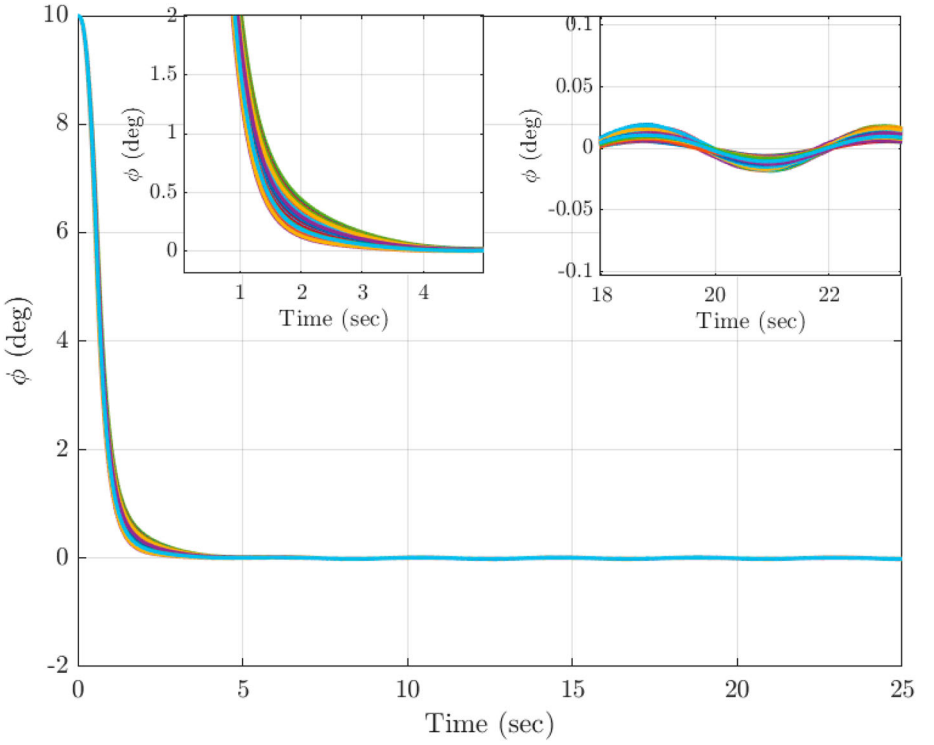

Figure 15. Time period variation based external disturbance impact on ϕ.

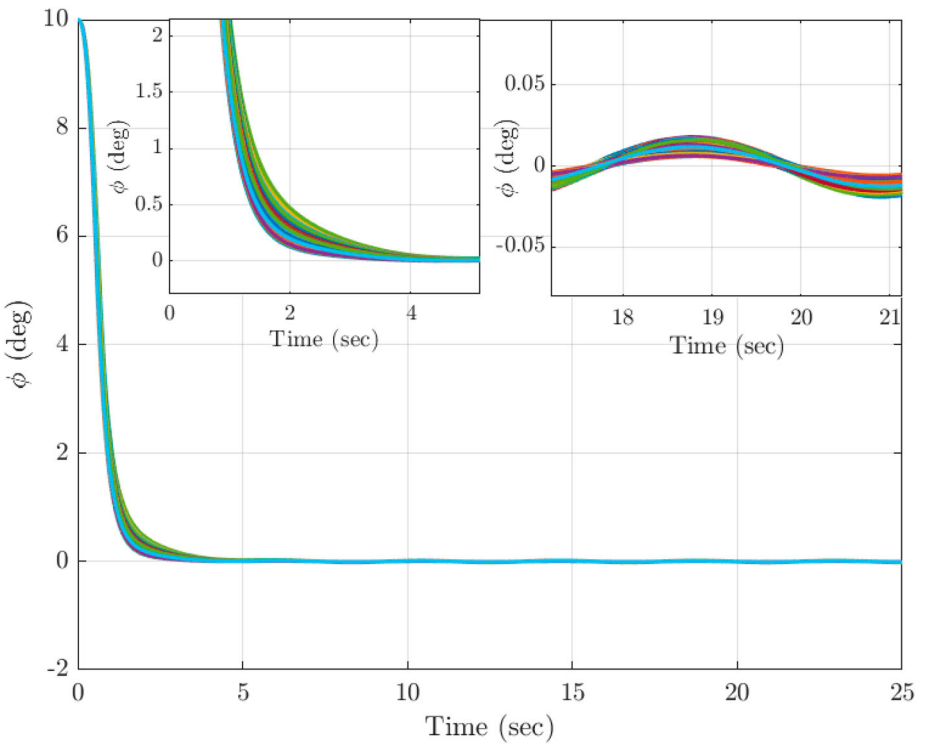

Figure 16. Amplitude variation based external disturbance impact on ϕ.

In the second simulation scenario, the amplitude of the sinusoidal White Gaussian disturbance is varied from 1 to 2.5 to assess the variation of roll angle. The results are depicted in Figure 16 and It is noteworthy that, in the case of the disturbed environmental scenario, the amplitude of 1 has been selected for the sinusoidal White Gaussian disturbance. Examination of the zoomed-in sections of Figure 16 reveals that the effects of the variation in amplitude on settling time and steady-state response are almost identical to the effects resulting from changes in

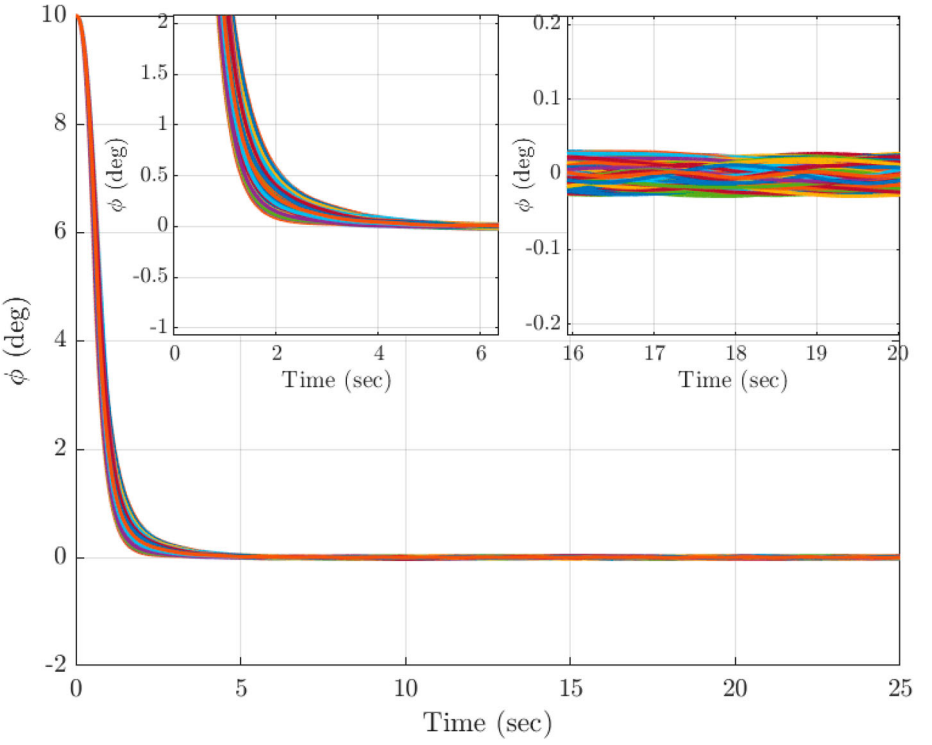

Figure 17. SNR variation based external disturbance impact on ϕ.

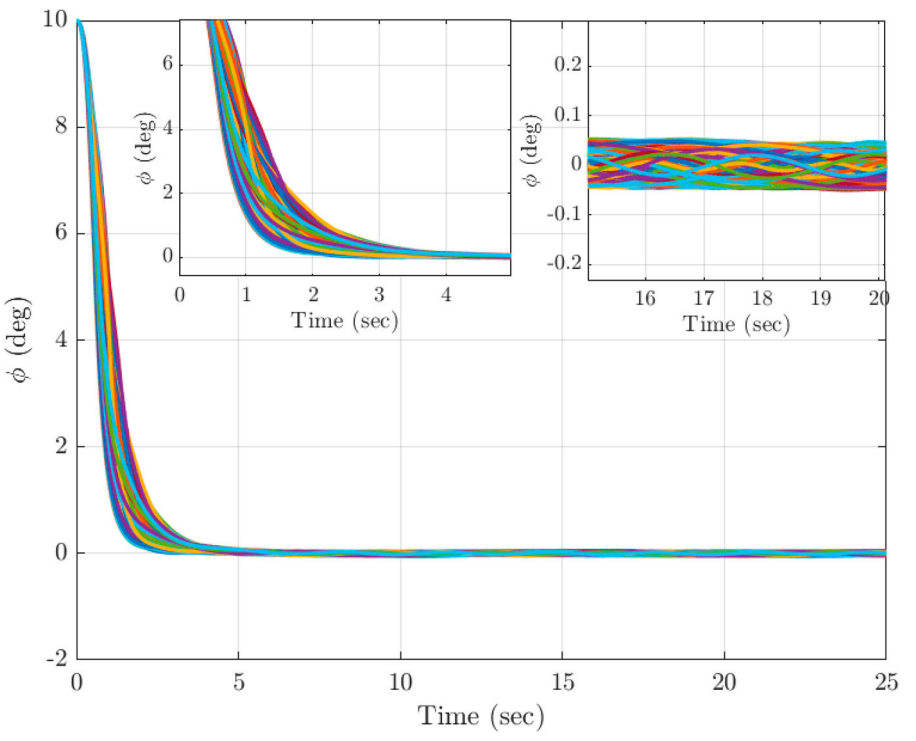

Figure 18. Combined variation based external disturbance impact on ϕ.

the time period of Figure 15, as discontinuous control remains consistent.

Figure 17 illustrates the roll angle response obtained due to variations in SNR with respect to the disturbances. The zoomed-in portion of the figure shows that, compared to Figures 15–16, the steady-state response tends to be less pulsating. Finally, for the sake of completeness, Figure 18 presents the combined effects of disturbances

on the proposed control scheme, considering factors such as time period, amplitude and SNR. The steady-state response can be achieved by adjusting the design gains of the discontinuous control within the scenarios outlined in the Monte Carlo simulations.

More significantly, the proposed control algorithm demonstrated asymptotic stability because of the remarkable consequences of the proposed tanh SOSMC in comparison with classical SOSMC and PID SOSMC. Owing to the suggested sliding surface and uncomplicated implementation, the proposed controller with a nonlinear sliding manifold proved to be a reliable choice to suppress the WRP in a perturbed environment.

5. Conclusion

In this paper, a robust nonlinear control strategy for dealing with the WRP has been proposed. The implementation of the robust nonlinear sliding manifold based SOSMC law and ROFPI observer reinforce the controller design. To estimate the side slip angle β, a ROFPI observer with a convergence function based on the equivalent control concept is employed, and a comparison between the ROPI observer and ROFPI observer is presented. The results demonstrate the fast convergence and error reduction in the case of the ROFPI observer. The sliding manifold of the proposed method is constructed by the *tanh* function that provides the system motion to be contained within this manifold, and eventually converges the roll angle to zero in finite time. The performance of the proposed SOSMC, classical SOSMC and PID SOSMC controllers is characterized by considering the WRP with identical switching law in perturbed and unperturbed environments. Additionally, a numerical comparison is made to investigate the performance of the aforementioned controllers, which highlights the superiority of the proposed controller. To ensure the effectiveness of the proposed controller, Monte Carlo simulations that account for variations in external disturbances have been conducted. The continuous control law can be developed further in relation to its design gains to maintain a steady-state response. In the future, we plan to incorporate the yaw angle and yaw rate into the wing rock dynamic model to formulate a nonlinear control scheme for the WRP. Additionally, the realization of the proposed controller on a WRP prototype is envisaged to further characterize the performance of the proposed controller in the near future.

Acknowledgments

The authors express their gratitude to the anonymous reviewers for their valuable suggestions in enhancing this paper.

Author contributions

(a) Ahmad Mahmood: Methodology, Software, Formal Analysis, Data Correction, Investigation, Original Draft Writing.
(b) Jamshed Iqbal: Conceptualization, Supervision, Validation, Project Administration, Resources, Review and Editing.

All authors have reviewed and approved the final version of the manuscript.

Data Availability Statement

Data supporting the findings of this study are available from the first author (Ahmad Mahmood) upon a reasonable request.

Disclosure statement

No potential conflict of interest was reported by the author(s).

Funding

This study is conducted without any funding.

References

Abdul-Kareem, A. I., Hasan, A. F., Al-Qassar, A. A., Humaidi, A. J., Hassan, R. F., Ibraheem, I. K., & Azar, A. T. (2022). Rejection of wing-rock motion in delta wing aircrafts based on optimal LADRC schemes with butterfly optimization algorithm. *Journal of Engineering Science and Technology*, *17*(4), 2476–2495.

Afifa, R., Ali, S., Pervaiz, M., & Iqbal, J. (2023). Adaptive backstepping integral sliding mode control of a mimo separately excited DC motor. *Robotics*, *12*(4), 105. https://doi.org/10.3390/robotics12040105

Ajwad, S. A., Iqbal, J., Khan, A. A., & Mehmood, A. (2015). Disturbance-observer-based robust control of a serial-link robotic manipulator using SMC and PBC techniques. *Studies in Informatics and Control*, *24*(4), 401–408. https://doi.org/10.24846/sic

Al-Qassar, A. A., Al-Obaidi, A. S. M., Hasan, A. F., Humaidi, A. J., A. R. Nasser, Alkhayyat, A., & Ibraheem, I. K. (2021). Finite-time control of wing-rock motion for delta wing aircraft based on whale-optimization algorithm. *Indonesian Journal of Science and Technology*, *6*(3), 441–456. https://doi.org/10.17509/ijost.v6i3

Andrievsky, B., Kudryashova, E. V., Kuznetsov, N. V., & Kuznetsova, O. A. (2020). Aircraft wing rock oscillations suppression by simple adaptive control. *Aerospace Science and Technology*, *105*, 106049. https://doi.org/10.1016/j.ast.2020.106049

Andrievsky, B., Kudryashova, E. V., Kuznetsov, N. V., Kuznetsova, O. A., Tomashevich, S., & Mokaev, T. N. (2019). Simple adaptive control of aircraft roll angle, suppressing the wing rock oscillations. *Mathematics in Engineering, Science & Aerospace (MESA)*, *10*(3), 106049.

Boutat, D., & Zheng, G. (2021). *Observer design for nonlinear dynamical systems*. Springer International Publishing.

Calise, A., Shin, Y., & Johnson, M. (2004, August). A comparison study of classical and neural network based adaptive control

of wing rock. In *AIAA Guidance, Navigation, and Control Conference and Exhibit* (p. 5320).

Cao, C., Hovakimyan, N., & Lavretsky, E. (2006, August). Application of L1 adaptive controller to wing rock. In *AIAA Guidance, Navigation, and Control Conference and Exhibit* (p. 6426).

Ding, S., Mei, K., & Yu, X. (2021). Adaptive second-order sliding mode control: A Lyapunov approach. *IEEE Transactions on Automatic Control*, *67*(10), 5392–5399. https://doi.org/10.1109/TAC.2021.3115447

Ene, C. (2013). Nonlinear control law design for lateral aircraft dynamics at high angles of attack. *Applied Mechanics and Materials*, *325-326*, 1210–1214. https://doi.org/10.4028/www.scientific.net/AMM

Fan, Y., Qiu, B., Liu, L., & Yang, Y. (2023). Global fixed-time trajectory tracking control of underactuated USV based on fixed-time extended state observer. *ISA Transactions*, *132*, 267–277. https://doi.org/10.1016/j.isatra.2022.06.011

Furat, M., & Eker, I. (2014). Second-order integral sliding-mode control with experimental application. *ISA Transactions*, *53*(5), 1661–1669. https://doi.org/10.1016/j.isatra.2014.05.030

Ghorawat, P. (2015). Adaptive, neural and robust control of Wing-Rock and aeroelastic system.

Guglieri, G., & Sartori, D. (2013). Design of a sliding mode control for wing rock suppression in highly-swept wing aircraft. *International Journal of Aerospace Sciences*, *2*(1), 1–10.

Hsu, C.-F., Lin, C.-M., & Chen, T.-Y. (2005). Neural-network-identification-based adaptive control of wing rock motions. *IEE Proceedings-Control Theory and Applications*, *152*(1), 65–71. https://doi.org/10.1049/ip-cta:20050904

Humaidi, A. J., Hameed, A. H., & Ibraheem, I. K. (2019, April). Design and performance study of two sliding mode backstepping control schemes for roll channel of delta wing aircraft. In *2019 6th International Conference on Control, Decision and Information Technologies (CoDIT)* (pp. 1215–1220). IEEE.

Ibrir, S., & Su, C. Y. (2014). Robust nonlinear feedback design for wing rock stabilization. *Journal of Guidance, Control, and Dynamics*, *37*(1), 321–325. https://doi.org/10.2514/1.61314

Kuperman, A., & Zhong, Q.-C. (2015). UDE-based linear robust control for a class of nonlinear systems with application to wing rock motion stabilization. *Nonlinear Dynamics*, *81*(1-2), 789–799. https://doi.org/10.1007/s11071-015-2029-x

Lee, K. W., & Singh, S. N. (2017). Immersion and invariance-based adaptive wing rock control with nonlinear terminal manifold. *Nonlinear Dynamics*, *88*(2), 955–972. https://doi.org/10.1007/s11071-016-3287-y

Lin, C. M., & Hsu, C. F. (2004). Supervisory recurrent fuzzy neural network control of wing rock for slender delta wings. *IEEE Transactions on Fuzzy Systems*, *12*(5), 733–742. https://doi.org/10.1109/TFUZZ.2004.834803

Liu, Z. L., Su, C. Y., & Svoboda, J. (2003, May). Control of wing rock using fuzzy PD controller. In *The 12th IEEE International Conference on Fuzzy Systems, 2003, FUZZ'03* (Vol. 1, pp. 414–419). IEEE.

Liu, Z. L., Su, C. Y., & Svoboda, J. (2004, June). Control of wing rock phenomenon with a variable universe fuzzy controller. In *Proceedings of the 2004 American Control Conference* (Vol. 2, pp. 1719–1724). IEEE.

Liu, Z., & Svoboda, J. (2003, June). Dutch-roll limit-cycle oscillations suppress using fuzzy sliding-mode control. In *2003 4th International Conference on Control and Automation Proceedings* (pp. 625–629). IEEE.

Mahmood, A. (2025). Control of wing aeroelastic system in presence of wind gust using logarithmic sliding mode control. *Journal of Vibration and Control*, 10775463241312815. https://doi.org/10.1177/10775463241312815

Mahmood, A., & Bhatti, A. I. (2023). Range guidance for subsonic unpowered gliding vehicle using integral action-based sliding mode control. *International Journal of Dynamics and Control*, *12*, 1–11.

Mahmood, A., & Okasha, M. (2024). Reduced-order sliding mode observer-based backstepping integral logarithmic sliding mode control: Application to wing aeroelastic system. *International Journal of Aeronautical and Space Sciences*, 1–12. https://doi.org/10.1007/s42405-024-00834-1

Mahmood, A., Okasha, M., & Saeed, A. (2024). Neural adaptive sliding mode control for camera positioner quadrotor UAV. *International Journal of Aeronautical and Space Sciences*, 1–15. https://doi.org/10.1007/s42405-024-00781-x

Malekzadeh, M., Khosravi, A., Rasouli, H., & Noei, A. R. (2015, November). Wing rock suppression via backstepping controller. In *2015 2nd International Conference on Knowledge-Based Engineering and Innovation (KBEI)* (pp. 792–796). IEEE.

Malekzadeh, M., Sadati, J., & Alizadeh, M. (2016). Adaptive PID controller design for wing rock suppression using self-recurrent wavelet neural network identifier. *Evolving Systems*, *7*(4), 267–275. https://doi.org/10.1007/s12530-015-9143-3

Mechali, O., Xu, L., Xie, X., & Iqbal, J. (2022). Fixed-time nonlinear homogeneous sliding mode approach for robust tracking control of multirotor aircraft: Experimental validation. *Journal of the Franklin Institute*, *359*(5), 1971–2029. https://doi.org/10.1016/j.jfranklin.2022.01.010

Midhat, B. F. (2017). Optimal LQR controller design for wing rock motion control in delta wing aircraft. *Engineering and Technology Journal*, *35*(5 Part A).473–478. https://doi.org/10.30684/etj.35.5A.6

Pakmehr, M. (2005). *Dynamic modelling and nonlinear control of vortex-coupled delta wing systems* [PhD diss.]. Concordia University.

Rong, H. J., Han, S., & Zhao, G. S. (2014). Adaptive fuzzy control of aircraft wing-rock motion. *Applied Soft Computing*, *14*, 181–193. https://doi.org/10.1016/j.asoc.2013.03.001

Roshanian, J., & Rahimzadeh, E. (2021). Novel model reference adaptive control with application to wing rock example. *Proceedings of the Institution of Mechanical Engineers, Part G: Journal of Aerospace Engineering*, *235*(13), 1911–1929. https://doi.org/10.1177/0954410020987041

Saad, A. A. (2000). *Simulation and analysis of wing rock physics for a generic fighter model with three degrees-of-freedom*. Air Force Institute of Technology.

Sreenatha, A. G., Nair, N. K., & Sudhakar, K. (2000). Aerodynamic suppression of wing rock using fuzzy logic control. *Journal of Aircraft*, *37*(2), 345–348. https://doi.org/10.2514/2.2602

Tao, C. W., Taur, J. S., Chang, C. W., & Chang, Y. H. (2012). Simplified type-2 fuzzy sliding controller for wing rock system. *Fuzzy Sets and Systems*, *207*, 111–129. https://doi.org/10.1016/j.fss.2012.02.015

Tewari, A. (2000). Nonlinear optimal control of wing rock including Yawing motion. In *18th Applied Aerodynamics Conference* (p. 4251).

Ullah, M. I., Ajwad, S. A., Irfan, M., & Iqbal, J. (2016). Non-linear control law for articulated serial manipulators: Simulation augmented with hardware implementation. *Elektronika Ir*

Elektrotechnika, *22*(1), 3–7. https://doi.org/10.5755/j01.eee.22.1.14094

Utkin, V. I. (2013). *Sliding modes in control and optimization*. Springer Science & Business Media.

Utkin, V., Poznyak, A., Orlov, Y., & Polyakov, A. (2020). Conventional and high order sliding mode control. *Journal of the Franklin Institute*, *357*(15), 10244–10261. https://doi.org/10.1016/j.jfranklin.2020.06.018

Utkin, V., Poznyak, A., Orlov, Y. V., & Polyakov, A. (2020). *Road map for sliding mode control design*. Springer International Publishing.

Wu, D., Chen, M., Gong, H., & Wu, Q. (2017). Robust backstepping control of wing rock using disturbance observer. *Applied Sciences*, *7*(3), 219. https://doi.org/10.3390/app7030219

Wu, D. W., Chen, M., Gong, H. J., & Ye, H. (2014, June). Control of wing rock based on high order sliding mode disturbance observer. In *Proceeding of the 11th World Congress on Intelligent Control and Automation* (pp. 873–878). IEEE.

Xin, M., & Balakrishnan, S. N. (2004). Control of the wing rock motion using a new suboptimal control method. *Proceedings of the Institution of Mechanical Engineers, Part G: Journal of Aerospace Engineering*, *218*(4), 257–266. https://doi.org/10.1243/0954410041872834

Yin, H., Zhang, X., Huang, X., & Lu, H. (2019). Two novel robust tracking control strategies for eliminating aircraft wing rock. *Proceedings of the Institution of Mechanical Engineers, Part G: Journal of Aerospace Engineering*, *233*(8), 3042–3055. https://doi.org/10.1177/0954410018794807

Zribi, M., Alshamali, S., & Al-Kendari, M. (2013). Suppression of the wing-rock phenomenon using nonlinear controllers. *Nonlinear Dynamics*, *71*(1-2), 313–322. https://doi.org/10.1007/s11071-012-0662-1